# Parameter calibration of a discrete element model for a mixture of cotton stalks and residual film

Jinming Li, Jiaxi Zhang*, Yichao Wang, Jiangtong Yu, Chunxiao Xing
(*College of Mechanical and Electrical Engineering, Xinjiang Agricultural University, Urumqi 830052, China*)

**Abstract:** To address the issue of insufficient accuracy in the discrete element simulation model for cotton stalk -residual film mixtures, this paper employs the Hertz-Mindlin model with the JKR contact model to calibrate the contact parameters. First, significant parameters affecting the angle of repose were identified using Plackett-Burman experiments. Subsequently, the optimal parameter range was determined in conjunction with the steepest climb test. A regression model was constructed using Box-Behnken experiments to optimize the parameters, yielding the optimal parameter combination: cotton stalk-residual film rolling friction coefficient of 0.46, residual film-residual film rolling friction coefficient of 0.31, residual film-steel rolling friction coefficient of 0.47, and residual film-residual film JKR surface energy of 0.41 J/m². Simulated pile-up tests were conducted on a mixture of cotton stalks and residual film using these optimal parameter combinations. The results showed that the error between the simulated and measured angle of repose was only 3.06%, validating the reliability of the parameters and providing a basis for research into the interaction characteristics between cotton stalks and residual film during film recovery.
**Keywords:** cotton stalk-residual plastic film mixture, parameter calibration, angle of repose, discrete element method
**DOI:** 10.25165/j.ijabe.20261903.10246

**Citation:** Li J M, Zhang J X, Wang Y C, Yu J T, Xing C X. Parameter calibration of a discrete element model for a mixture of cotton stalks and residual film. Int J Agric & Biol Eng, 2026; 19(3): 80–88.

## 1 Introduction

In 2024, Xinjiang's cotton production reached 5.686 Mt, yielding approximately 28.43 Mt of cotton straw[1]. Rich in nitrogen, phosphorus, potassium, and trace elements, cotton straw represents a valuable resource. However, burning or discarding it leads to significant resource waste and environmental pollution[2]. Current utilization methods for cotton straw include fertilization, feed conversion, raw material sourcing, substrate conversion, and fuel conversion. Specifically, fertilizing with cotton stalks can boost cotton yields by an average of about 10% per mu. Using stalk for feed reduces costs by 20%-40%. Fuel utilization enables the production of solid fuels, gasification, and power generation, while raw material applications range from construction materials and light industry to textile feedstock. Substrate utilization is primarily for edible fungus cultivation or growth media[3]. In Xinjiang, the dominant method for cotton stalk utilization, accounting for over 50% of the total, is direct shredding and returning it to fields as fertilizer[4]. However, existing combined machinery for shredding cotton stalks and recovering residual film mixes these materials during operation. This practice results in excessively high impurity levels in the recovered cotton stalks. Consequently, the recovered film is often unusable for direct processing, limiting its resource utilization potential. To thoroughly investigate the interaction mechanisms between residual film and cotton stalks, precise contact parameters for the cotton stalk-residual film mixture are essential. However, the complex interaction properties of this composite material, combined with the errors introduced by traditional physical measurement methods, have a significant impact on the accuracy of subsequent modeling and simulation. The Discrete Element Method (DEM), a microscopic approach that quantifies particle interaction mechanisms, offers an ideal solution for studying contact parameters between cotton stalks and residual film[5]. Therefore, obtaining precise parameters through discrete element simulation not only provides a theoretical basis for understanding the interaction between cotton straw and residual film, but also lays a crucial foundation for developing more complex models of the cotton straw-residual film-soil complex.

The Discrete Element Method (DEM) has become a mature tool for studying the mechanical behavior of agricultural materials, with applications ranging from modeling single components to complex mixtures[5]. Research focusing on single-material modeling has achieved considerable depth. For instance, Shi et al.[6] developed a DEM bonding model for flexible flax stems and calibrated its parameters by simulating the shearing process. Du et al.[7] constructed a DEM mechanical model of tea plant stems, conducting tensile and puncture tests. Zhang et al.[8] used Xinjiang cotton stalks as their test material, employing EDEM software for experimental simulation, parameter calibration, and validation through crushing tests. Shu et al.[9] focused on rapeseed residues at optimal maturity after combine harvesting. They utilized EDEM simulation software for contact parameter calibration of major components and performed DEM-CFD coupled gas-solid analysis of a cyclone separation and cleaning device for rapeseed combine harvesting, integrated with bench testing. Shen et al.[10] investigated residual plastic film in cotton field tillage layers. Using EDEM software and the Hertz-Mindlin with Bonding contact model, they calibrated parameters for the film's discrete element model. The model's validity was confirmed by comparing stretching process

**Received date:** 2025-10-03 **Accepted date:** 2026-05-31
**Biographies: Jinming Li**, PhD candidate, research interest: recycling agriculture technology and equipment, Email: xjaujinmingli@163.com; **Yichao Wang**, PhD, research interest: harvesting machinery, Email: 360318122@qq.com; **Jiangtong Yu**, PhD, research interest: recycling of agricultural technology and equipment, Email: yujtong@163.com; **Chunxiao Xing**, PhD, research interest: recycling agriculture technology and equipment, Email: xcx@xjau.edu.cn.
***Corresponding author: Jiaxi Zhang**, Professor, research interest: recycling of agricultural technology and equipment. College of Mechanical and Electrical Engineering, Xinjiang Agricultural University, Urumqi 830052, China. Tel: +86-13899961137, Email: zhangjiaxi@xjau.edu.cn.

states and strain curves from physical tests with simulation results. Li et al.[11] proposed a multi-feature integrated analysis method for constructing discrete element models of film-like materials, considering flexible deformation, friction properties, and aerodynamic characteristics. They developed a residual film DEM model using the Shell model in Rocky simulation software and validated its reliability through material flow experiments. Liu et al.[12] employed the Bonding-V2 model with API rapid filling technology to establish a DEM simulation model for the residual film-soil-root-straw composite system. Deng et al.[13] developed a residual film DEM to investigate morphological changes during the operation of a tubular fertilizer applicator. Fang et al.[14] created a DEM for residual film in the tillage layer, validated by tensile tests. Tian et al.[15] used the Moving Element Method (MEM) to model corn stover-soil mixtures, calibrating contact parameters based on the angle of repose. Ma et al.[16] applied DEM to develop a simulation model for corn stover-cow manure mixtures, validating parameters through uniaxial compression tests. Despite these advancements, which have laid a solid foundation for DEM applications in agriculture, systematic research on discrete element simulation and parameter calibration specifically for cotton stalk-residual film mixtures remains a significant gap.

This study precisely calibrates the discrete element (DEM) contact parameters for cotton stalk-residual film mixtures found in Xinjiang cotton fields. Combining physical experiments with EDEM simulations, we used the measured physical angle of repose as the primary response variable for calibration[17]. A systematic optimization approach was implemented, incorporating Plackett-Burman screening to identify significant parameters, followed by the steepest ascent method to determine optimal parameter ranges. Finally, Box-Behnken response surface experiments were employed to establish the optimal parameter combination. The reliability of the calibrated parameters was validated through physical angle-of-repose tests. These research findings may serve as a reference for the development of a cotton stalk–residual film–soil complex model and for studies on the interaction characteristics between cotton stalks and residual film.

## 2 Materials and methods

### 2.1 Test materials

The experimental materials for this study comprised a mixture of cotton stalks and residual plastic film collected from Xinjiang cotton fields after the autumn harvest. To prepare simulated samples, the collected mixture was first separated. The moisture content of cotton stalks was determined using a drying method; after drying, the stalks were sorted, and those measuring 30 mm in length were selected, as samples within this length range accounted for 42% of the total. The residual plastic film was thoroughly cleaned and cut into small strips. Following separation, the densities of both the cotton stalks and residual plastic film were measured individually. Figure 1 displays the prepared samples and their corresponding simulated models.

### 2.2 Test method

A combined approach of simulation and physical testing was employed to calibrate the relevant parameters of the cotton stalk-residual film mixture. Specifically, the physical testing of the mixture's angle of repose was conducted using a dedicated angle-of-repose testing rig, which measured the actual mean angle of repose of the cotton stalk-residual film mixture[18]. Simulation tests for the angle of repose of cotton stalk-residual flim mixtures were carried out using EDEM 2022 software. Subsequently, Design-Expert 13.0 software was utilized for a Plackett-Burman screening experimental design[19]. Significance analysis was then performed on the Plackett-Burman test results to identify the parameters that significantly influenced the simulated angle of repose of the cotton stalk-plastic film mixture. The optimal range for these significant factors was determined through steepest ascent experiments. A regression model for the significant factors affecting the pile angle of the cotton stalk-residual film mixture was subsequently established using a Box-Behnken experimental design[20]. The Optimization module was then employed to comprehensively optimize the parameters, resulting in the identification of the optimal parameter combination. Finally, simulation tests were conducted using this optimal parameter combination to compare the simulated angle of repose of the cotton stalk-residual film mixture with its actual measured angle of repose[21], thereby validating the accuracy of the calibrated parameters.

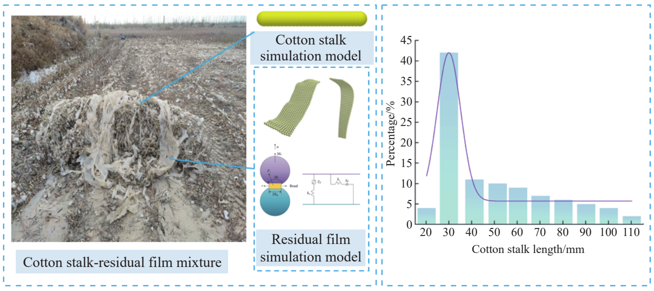


a. Discrete element model for cotton stalks and residual film
b. Proportion of cotton stalk length

Figure 1 Cotton stalk-residual film mixed material

### 2.3 Determination of intrinsic material parameters

#### 2.3.1 Determination of intrinsic parameters of cotton stalks

Cotton stalks of the Xinluzao 66 variety were collected from Yuli County, Bayingolin Mongol Autonomous Prefecture, Xinjiang Uygur Autonomous Region, and used as experimental material. To accurately determine their physical and mechanical properties, ten stalk samples were randomly selected for processing and classification. During parameter measurement, the diameter at the midpoint of each stalk was first measured using a Vernier caliper. Moisture content was determined using an electronic balance and a drying oven. Subsequently, a universal testing machine was employed to conduct a three-point bending compression test on the stalks (apparatus illustrated in Figure 2a). The loading rate was set at 2 mm/min and maintained until specimen failure. Throughout the testing process, the universal testing machine recorded load-displacement data (curve depicted in Figure 2b). Concurrently, a Vernier caliper measured diameter deformation in both the compression direction and the perpendicular direction. This test was repeated 10 times. Mechanical parameters were calculated using Equation (1) and then averaged. The final measured mean shear modulus for the cotton stalk was 650 MPa.

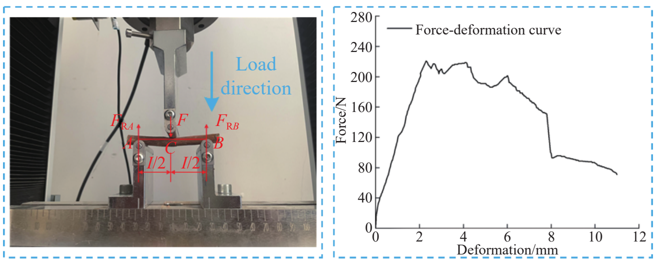


a. Cotton stalk bending test
b. Compression load-displacement curve

Figure 2 Determination of cotton stalk characteristic parameters

$$\begin{cases} E = \dfrac{FL^3}{48I\delta} \\ I = \dfrac{bh^3}{12} \\ G = \dfrac{E}{2(1+\mu)} \end{cases} \tag{1}$$

where, $E$ is the elastic modulus, Pa; $F$ is the applied load, N; $L$ is the support span, m; $I$ is the sectional moment of inertia, m$^4$; $\delta$ is the deflection, m; $b$ is the specimen width, m; $h$ is the specimen height, m; $G$ is the shear modulus, Pa; and $\mu$ is the Poisson's ratio.

2.3.2 Determination of intrinsic parameters of residual film

To investigate the mechanical properties of the residual film, the film was first cleaned, dried, and cut into standard specimens. Subsequently, mechanical property testing was conducted in accordance with GB/T 1040.3-2006. Tensile tests were performed on the specimens using a TMS texture analyzer (apparatus illustrated in Figure 3). The test parameters were set as follows: a loading rate of 200 mm/min, with loading ceasing upon specimen fracture. Each test series was repeated 10 times to ensure data reliability. Finally, Poisson's ratio, elastic modulus, and shear modulus were calculated using Equation (2). The results indicated an average shear modulus of 1.57 MPa for the residual film. The intrinsic parameters of cotton stalks and residual film are shown in Table 1.

$$\begin{cases} E = \dfrac{\sigma}{\varepsilon} \\ \sigma = \dfrac{F}{A_0} \\ \varepsilon = \dfrac{\Delta L}{L_0} \\ G = \dfrac{E}{2(1+\mu)} \end{cases} \tag{2}$$

where, $E$ is the elastic modulus, Pa; $\delta$ is the stress, Pa; $\varepsilon$ is the strain; $F$ is the tensile load, N; $\Delta L$ is the specimen elongation, m; $L_0$ is the original gauge length of the specimen, m.

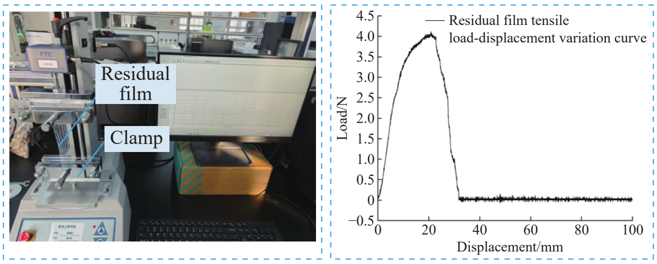


a. Residual film tensile test b. Tensile load-displacement curve

Figure 3 Determination of residual film characteristic parameters

**Table 1 Material intrinsic parameters**

| Parameters | Value |
|---|---|
| Cotton stalk Poisson's ratio | 0.35 |
| Cotton stalk shear modulus/MPa | 650 |
| Residual film Poisson's ratio | 0.32 |
| Residual film shear modulus/MPa | 1.57 |
| Steel Poisson's ratio | 0.3 |
| Steel shear modulus/MPa | $7.8\times10^4$ |
| Steel density/kg·m$^{-3}$ | 7850 |

### 2.4 Contact parameter determination

2.4.1 Determination of static friction coefficient between cotton stalk and steel plate

This study aims to determine the static friction coefficient between cotton stalks and between cotton stalks and steel. Experiments were conducted using a homemade inclined plane apparatus. During testing, cotton stalks were placed on the base plate of the apparatus, and the incline angle was gradually increased until the sample stalks were on the verge of slipping. The critical angle at this point was recorded[22]. Each set of experiments was repeated 10 times. The average measured angle was then substituted into Equation (3) to calculate the static friction coefficient.

$$\mu = \tan\varphi \tag{3}$$

where, $\mu$ represents the coefficient of static friction; $\varphi$ denotes the angle of inclination of the inclined plane during sliding, (°).

To determine the static friction coefficient between cotton stalks, the base plate of the inclined plane apparatus was covered with cotton stalks, and the aforementioned test procedure was repeated. The static friction coefficient between cotton stalks and steel was measured to be 0.40, while that between cotton stalks alone was 0.51.

2.4.2 Determination of rolling friction coefficient between cotton stalks and steel plate

To determine the rolling friction coefficient between cotton stalks and a steel plate, this study employed the inclined plate rolling method. An experimental platform, as illustrated in Figure 4, was constructed for this purpose. During testing, the steel inclined plate was first fixed at a specific angle $\theta$. A cotton stalk sample was then released from rest at a vertical height $H$ above the inclined surface[22]. After the sample rolled down the incline and came to rest on the horizontal plate, its rolling distance $S$ on the horizontal plate was precisely measured. This distance was subsequently used to calculate the rolling friction coefficient.

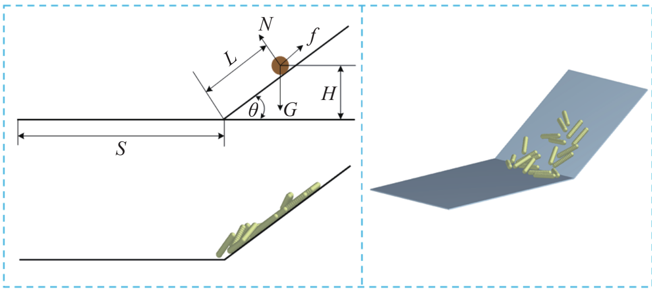


a. Principle of rolling friction measurement b. Simulation test

Figure 4 Rolling friction coefficient measurement

If the tilt angle $\theta$ and slope length $L$ are excessively large, the sample is prone to bounce during rolling, which can compromise the accuracy of the results. Conversely, if these parameters are too small, the horizontal rolling distance becomes unacceptably short, leading to an increased relative measurement error. Assuming the sample undergoes purely rolling motion solely under the influence of rolling friction, the law of conservation of energy yields:

$$GH = \mu_f G(L\cos\theta + S) \tag{4}$$

where, $\mu_f$ is the rolling friction coefficient between cotton stalks and steel plate; $G$ is the gravitational force of cotton stalks, N.

The test was repeated 10 times, and the average values were calculated. The measured rolling friction coefficient between cotton stalks and steel was found to be 0.06, while the coefficient between cotton stalks themselves was 0.2.

## 3 Angle of repose simulation test

### 3.1 Contact model selection

The adhesion observed between cotton stalks and residual film stems from the film's inherent static properties and the fragmentation of cotton stalks after shredding and their return to the field. The Hertz-Mindlin with JKR contact model is capable of representing the mutual attraction between particles[23]. Consequently, this study utilizes the Hertz-Mindlin with JKR Cohesion (JKR) model to construct a discrete element model for the cotton stalk-residual film mixture. Contact occurs due to particle motion, during which particle surfaces gradually deform to generate contact forces. The normal elastic contact force, $F_{\text{JKR}}$, within the JKR model is dependent on the overlap, $\delta$, the interaction parameter, $\gamma$, and the surface energy. It is calculated as follows:

$$\begin{cases} F_{\text{JKR}} = -4\sqrt{\pi\gamma E^*}\alpha^{\frac{3}{2}} + \dfrac{4E^*}{3R^*}\alpha^3 \\ \delta = \dfrac{\alpha^2}{R^*} - \sqrt{\dfrac{4\pi\gamma\alpha}{E^*}} \end{cases} \tag{5}$$

Among them:

$$\frac{1}{E^*} = \frac{1-v_1^2}{E_1} + \frac{1-v_2^2}{E_2} \tag{6}$$

$$R^* = \frac{1}{R_1} - \frac{1}{R_2} \tag{7}$$

where, $F$ is the normal elastic force in the JKR model, N; $\delta$ is the normal overlap between two contacting particles, m; $\alpha$ is the tangential overlap between two contacting particles, m; $\gamma$ is the surface energy, N/m; $E^*$ is the equivalent Young's modulus, Pa; $R^*$ is the equivalent contact radius, m; $v_1$ and $v_2$ are the Poisson's ratios of the two particles; $E_1$ and $E_2$ are the shear moduli of the two contacting particles, Pa; $R_1$ and $R_2$ are the radii of the two contacting particles, m.

When the surface energy $\gamma = 0$, the normal force $F_n$ in the $F_{\text{JKR}}$ model is equal to that in the Hertz-Mindlin contact model:

$$F_{\text{JKR}} = F_n = \frac{4}{3}E^*\sqrt{R^*}\delta^{\frac{3}{2}} \tag{8}$$

If particles are not in direct contact, the JKR model can also provide attractive cohesive forces[24], with the maximum gap for non-zero cohesive forces between particles being:

$$\delta_c = \frac{\alpha_c^2}{R^*} - \sqrt{\frac{4\pi\gamma\alpha_c}{E^*}} \tag{9}$$

$$\alpha_c = \left[\frac{9\pi\gamma R^*}{2E^*} - \left(\frac{3}{4} - \frac{1}{\sqrt{2}}\right)\right]^{\frac{1}{3}} \tag{10}$$

where, $\delta_c$ represents the maximum normal gap between particles when non-zero cohesive forces exist, m; $\alpha_c$ denotes the maximum tangential gap between particles when non-zero cohesive forces exist, m.

When $\delta > \delta_c$, the cohesive force between particles becomes zero.

When particles are not in actual contact and the separation equals $\delta_c$, the cohesive force reaches its maximum value.

$$F_{pull\text{-}off} = -\frac{3}{2}\pi\gamma R^* \tag{11}$$

where, $F_{pull\text{-}off}$ is the cohesive force between two particles, N.

### 3.2 Simulation model development

3.2.1 Physical tests on angle of repose

To determine the angle of repose parameters for the cotton stalk-residual film mixture, this study developed a physical testing platform, as illustrated in Figure 5. The platform is principally composed of a hopper, a support frame, and a horizontal steel plate. During the test, the mixed material was loaded into the hopper and allowed to fall freely under gravity, forming a pile on the steel plate surface[25]. After the material pile reached a stable configuration, an angle measuring instrument was employed to record its naturally formed angle of repose. To ensure data reliability, the experiment was replicated 10 times independently, and the arithmetic mean of the measurement results was calculated. The statistical analysis revealed that the angle of repose for this mixed material is 31.59°.

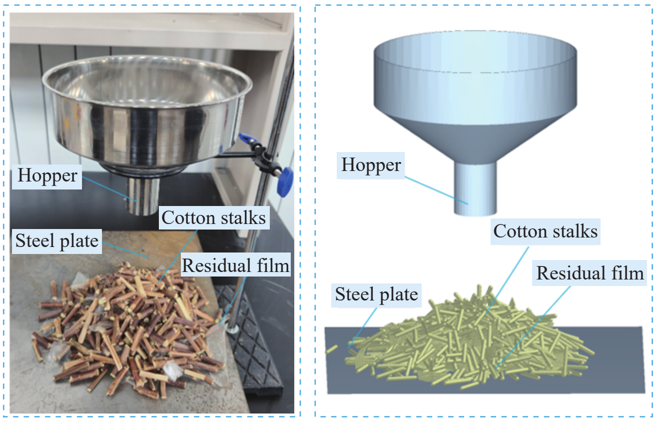


a. Physical test b. Simulation test

Figure 5 Simulation model of stacking angle

3.2.2 Simulation model establishment and EDEM parameter configuration

This study investigates the pile formation behavior of cotton stalk-residual film mixtures through numerical simulation using the EDEM software. The simulation employs the Hertz-Mindlin with JKR contact model. To strike a balance between simulation efficiency and model fidelity, cotton stalks were simplified into a model that replicates their physical dimensions, represented as a collection of circular particles. To accurately capture the flexible mechanical properties of residual film, it was modeled as strip-like elements and constructed using the bonding model. The geometric configuration of the simulation environment, including the hopper and steel plate, precisely mirrored the physical test setup. Particles were introduced at a rate of 5 kg/s via a particle generator, with a mass ratio of 77.19% cotton stalks to 22.81% residual film. The total simulation duration was 6.5 seconds, with the time step set to 20% of the Rayleigh time step and the mesh size set to three times the particle radius[26]. Once the particles formed a stable pile under gravity (as illustrated in Figure 6), Matlab-based image processing techniques were utilized on the simulation screenshots for binarization and contour line extraction[27]. Finally, linear fitting of the extracted contour data using Origin software yielded the simulated angle of repose for this mixed material. The physical parameter ranges for the cotton stalk-residual film mixture were determined based on preliminary experiments and referencing parameter ranges from studies[8,10,13,14], as detailed in Table 2.

## 4 Simulation tests and results analysis of residual film-cotton stalk mixtures

### 4.1 Plackett-Burman test and significance analysis

To rapidly identify the key factors influencing the angle of repose of cotton stalk-residual film mixtures, this study utilized the Plackett-Burman design method[26]. Experiments were designed and analyzed using Design-Expert, with the mixture's angle of repose serving as the response variable. This method assesses significance by comparing the differences in main effects across two levels for

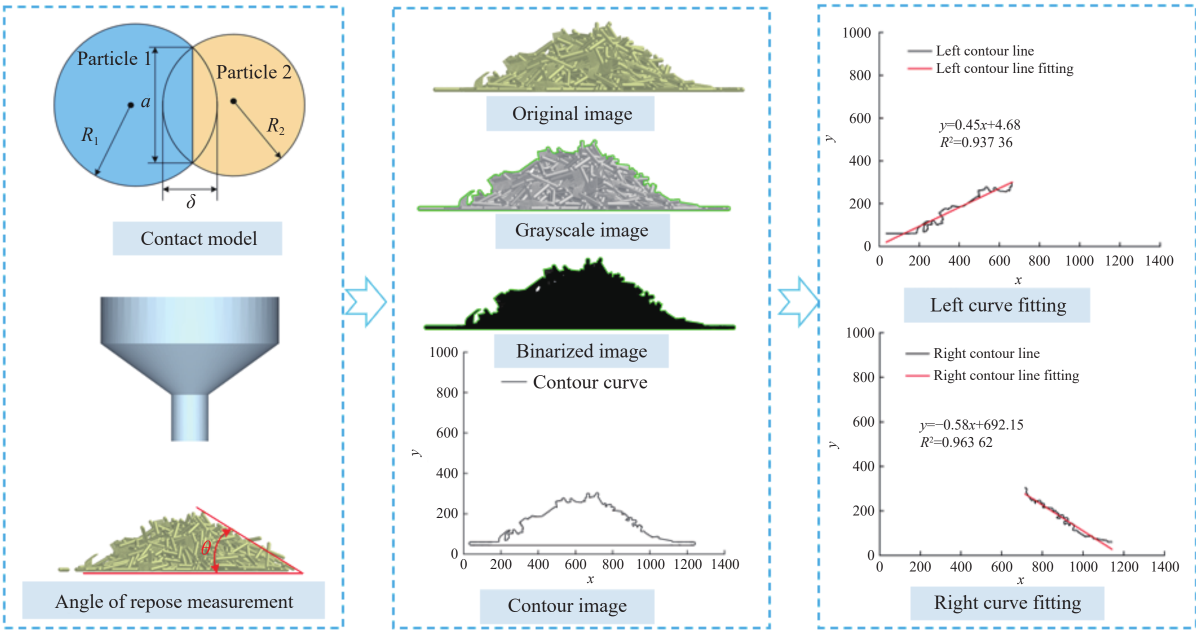


Figure 6 Fitting of the angle of repose profile

**Table 2 Simulation parameters for the angle of repose of a mixture of residual film and cotton stalk**

| Parameters | Values |
|---|---|
| Cotton stalk-cotton stalk recovery coefficient | 0.5 |
| Cotton stalk-static friction coefficient of cotton stalk | 0.51 |
| Cotton stalk-rolling friction coefficient of cotton stalk | 0.2 |
| Cotton stalk-steel recovery coefficient | 0.5 |
| Cotton stalk-static friction coefficient of steel | 0.4 |
| Cotton stalk-rolling friction coefficient of steel | 0.06 |
| Cotton stalk-residual film recovery coefficient $X_1$ | 0.3-0.5 |
| Cotton stalk-residual film static friction coefficient $X_2$ | 0.15-0.55 |
| Cotton stalk-residual film rolling friction coefficient $X_3$ | 0.2-0.8 |
| Residual film-residual film recovery coefficient $X_4$ | 0.34-0.74 |
| Residual film-residual film static friction coefficient $X_5$ | 0.25-0.85 |
| Residual film-residual film rolling friction coefficient $X_6$ | 0.2-0.6 |
| Residual film-static friction coefficient of steel $X_7$ | 0.32-0.72 |
| Residual film-rolling friction coefficient of steel $X_8$ | 0.2-0.8 |
| Cotton stalk-residual film JKR surface energy $X_9$/J·m$^{-2}$ | 0.1-0.5 |
| Residual film-residual film JKR surface energy $X_{10}$/J·m$^{-2}$ | 0.3-0.7 |

each factor. Table 3 lists the level codes for the experimental factors ($X_1$-$X_{10}$), while Tables 4 and 5 provide detailed experimental design schemes, results, and analyses of variance.

According to the ANOVA results in Table 5, four parameters significantly influenced the mixture's angle of repose ($p$<0.05) among all investigated factors: the cotton stalk-residual film rolling friction coefficient ($X_3$), residual film-residual film rolling friction coefficient ($X_6$), residual film-steel rolling friction coefficient ($X_8$), and residual film-residual film JKR surface energy ($X_{10}$). The cumulative contribution rate of these four factors reached as high as 91.89%[28], making them the dominant factors influencing changes in the angle of repose. Consequently, these four parameters were selected for subsequent steep slope climbing tests.

**Table 3 Plackett-Burman test factors and codes**

| Factor | Code | | |
|---|---|---|---|
| | −1 | 0 | 1 |
| Cotton stalk-residual film recovery coefficient $X_1$ | 0.3 | 0.4 | 0.5 |
| Cotton stalk-residual film static friction coefficient $X_2$ | 0.15 | 0.35 | 0.55 |
| Cotton stalk-residual film rolling friction coefficient $X_3$ | 0.2 | 0.50 | 0.8 |
| Residual film-residual film recovery coefficient $X_4$ | 0.34 | 0.54 | 0.74 |
| Residual film-residual film static friction coefficient $X_5$ | 0.25 | 0.55 | 0.85 |
| Residual film-residual film rolling friction coefficient $X_6$ | 0.2 | 0.4 | 0.6 |
| Residual film-static friction coefficient of steel $X_7$ | 0.32 | 0.52 | 0.72 |
| Residual film-rolling friction coefficient of steel $X_8$ | 0.2 | 0.5 | 0.8 |
| Cotton stalk-residual film JKR surface energy $X_9$/J·m$^{-2}$ | 0.1 | 0.3 | 0.5 |
| Residual film-residual film JKR surface energy$X_{10}$/J·m$^{-2}$ | 0.3 | 0.4 | 0.7 |

**Table 4 Plackett-Burman test design and results**

| Test No. | Factor | | | | | | | | | | | Angle of repose/(°) |
|---|---|---|---|---|---|---|---|---|---|---|---|---|
| | $X_1$ | $X_2$ | $X_3$ | $X_4$ | $X_5$ | $X_6$ | $X_7$ | $X_8$ | $X_9$ | $X_{10}$ | $K$ | |
| 1 | 1 | 1 | −1 | −1 | −1 | 1 | −1 | 1 | 1 | −1 | 1 | 33.68 |
| 2 | −1 | 1 | 1 | −1 | 1 | 1 | 1 | −1 | −1 | −1 | 1 | 31.88 |
| 3 | −1 | 1 | 1 | 1 | −1 | −1 | −1 | 1 | −1 | 1 | 1 | 32.89 |
| 4 | −1 | −1 | −1 | 1 | −1 | 1 | 1 | −1 | 1 | 1 | 1 | 34.88 |
| 5 | −1 | 1 | −1 | 1 | 1 | −1 | 1 | 1 | 1 | −1 | −1 | 28.07 |
| 6 | 1 | 1 | 1 | −1 | −1 | −1 | 1 | −1 | 1 | 1 | −1 | 32.13 |
| 7 | −1 | −1 | 1 | −1 | 1 | 1 | −1 | 1 | 1 | 1 | −1 | 35.72 |
| 8 | 1 | −1 | 1 | 1 | −1 | 1 | 1 | 1 | −1 | −1 | −1 | 34.21 |
| 9 | −1 | −1 | −1 | −1 | −1 | −1 | −1 | −1 | −1 | −1 | −1 | 25.12 |
| 10 | 1 | −1 | 1 | 1 | 1 | −1 | −1 | −1 | 1 | −1 | 1 | 27.44 |
| 11 | 1 | 1 | −1 | 1 | 1 | 1 | −1 | −1 | −1 | 1 | −1 | 34.18 |
| 12 | 1 | −1 | −1 | −1 | 1 | −1 | 1 | 1 | −1 | 1 | 1 | 29.23 |

**Table 5 ANOVA result**

| Parameters | Effect | $F$-value | $p$-value | Contribution | Order of significance |
|---|---|---|---|---|---|
| $X_1$ | 0.39 | 16.42 | 0.1540 | 0.36 | 8 |
| $X_2$ | 1.04 | 119.46 | 0.0581 | 2.59 | 5 |
| $X_3$ | 1.52 | 255.44 | 0.0398* | 5.54 | 3 |
| $X_4$ | 0.65 | 47.05 | 0.0922 | 1.02 | 7 |
| $X_5$ | −1.07 | 125.68 | 0.0566 | 2.72 | 10 |
| $X_6$ | 4.95 | 2709.48 | 0.0122* | 58.72 | 1 |
| $X_7$ | 0.23 | 5.78 | 0.2510 | 0.13 | 9 |
| $X_8$ | 1.36 | 205.44 | 0.0443* | 4.45 | 4 |
| $X_9$ | 0.74 | 59.86 | 0.0818 | 1.30 | 6 |
| $X_{10}$ | 3.11 | 1068.26 | 0.0195* | 23.15 | 2 |

To visually assess the influence of each factor, graphical analysis was performed on the Plackett-Burman experimental results, yielding a semi-normal probability effect plot (Figure 7a) and a Pareto chart (Figure 7b). In the semi-normal probability effect plot, the distance of effect points from the fitted line reflects their significance. Figure 7a shows that the effect points for $X_6$ (Residual Film-Residual Film Rolling Friction Coefficient) and $X_{10}$ (Residual Film-Residual Film JKR Surface Energy) deviate significantly from the fitted line, indicating highly significant positive effects on the angle of repose, with $X_6$ being more significant than $X_{10}$. The Pareto chart (Figure 7b) further validates and supplements this conclusion. It shows that the standardized effect values for factors $X_3$, $X_6$, $X_8$, and $X_{10}$ all exceed the significance threshold ($t$-value), reaffirming their significant positive influence on the angle of repose. Based on this analysis, these four significant factors were selected for subsequent steepest climb tests. The remaining non-significant factors will be fixed at their central levels: $X_1$=0.4, $X_2$=0.35, $X_4$=0.54, $X_5$=0.55, $X_7$=0.52, and $X_9$=0.3.

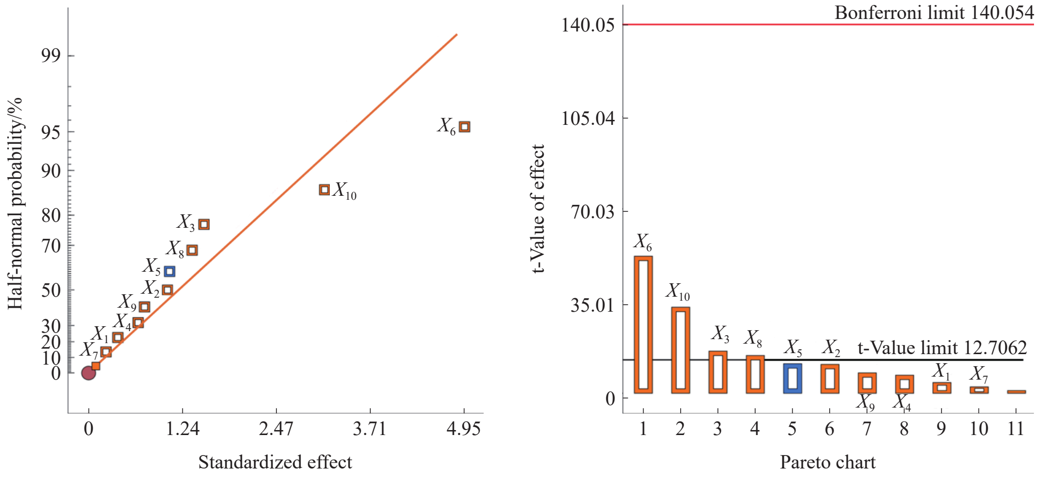


a. Standardized effect semi-normal probability plot

b. Pareto chart

Figure 7 Effect analysis

## 4.2 Steepest climb test design

Test results indicate a positive correlation between increasing levels of the four factors and the angle of repose. Concurrently, the relative error between simulated and experimental values exhibits a gradually increasing trend. At test group 1 ($X_3$=0.2, $X_6$=0.2, $X_8$=0.2, $X_{10}$=0.3 J/m$^2$), the relative error reached its minimum value of 4.18%, suggesting that the optimal parameter combination lies near this point. To achieve more precise optimization within this region, a Box-Behnken design (BBD) was employed for response surface analysis. Integrating the results from test groups 2 and 3, a new central point was selected near the minimum error point: cotton stalk-residual film rolling friction coefficient $X_3$=0.35, residual film-residual film rolling friction coefficient $X_6$=0.3, residual film-steel rolling friction coefficient $X_8$=0.35, and residual film-residual film JKR surface energy $X_{10}$=0.4 J/m$^2$. This point served as the basis for the subsequent four-factor, three-level experimental design, the experimental schedule is shown in Table 6.

Table 6 Test design and results of the steepest climb

| Test No. | $X_3$ | $X_6$ | $X_8$ | $X_{10}$ | Angle of repose/(°) | Relative error/% |
|---|---|---|---|---|---|---|
| 1 | 0.2 | 0.2 | 0.2 | 0.3 | 30.27 | 4.18 |
| 2 | 0.35 | 0.3 | 0.35 | 0.4 | 33.94 | 7.44 |
| 3 | 0.5 | 0.4 | 0.5 | 0.5 | 34.25 | 8.42 |
| 4 | 0.65 | 0.5 | 0.65 | 0.6 | 36.68 | 16.11 |
| 5 | 0.8 | 0.6 | 0.8 | 0.7 | 37.59 | 18.99 |

## 4.3 Box-Behnken experimental design

To precisely investigate the nonlinear relationship between the four significant factors ($X_3$, $X_6$, $X_8$, $X_{10}$) and the angle of repose, this study employed the Box-Behnken design (BBD) method[29]. Design-Expert software was utilized for experimental design and data analysis. Based on the experimental results, a quadratic polynomial regression model was constructed with the angle of repose as the response variable. Detailed factor coding, the experimental design plan, and the response results are presented in Tables 7 and 8, respectively.

Table 7 BBD test factors and levels coding

| Code | Factor | | | |
|---|---|---|---|---|
| | $X_3$ | $X_6$ | $X_8$ | $X_{10}$/J·m$^{-2}$ |
| –1 | 0.2 | 0.2 | 0.2 | 0.3 |
| 0 | 0.35 | 0.3 | 0.35 | 0.4 |
| 1 | 0.5 | 0.4 | 0.5 | 0.5 |

## 4.4 Regression model

Multivariate regression analysis was performed on the experimental data to establish a second-order regression model relating the angle of repose of the residual film-cotton stalk mixture to the four significant parameters. The equation is as follows:

$$Y = 29.35 + 1.96X_3 - 2.06X_6 + 3.74X_{10} - 2.29X_3X_8 - 2.41X_3X_{10} - 2.58X_6X_{10} - 2.75X_8X_{10} + 1.63X_6^2 + 2.86X_8^2 \quad (12)$$

Table 9 presents the results of the variance analysis for the regression model. These findings demonstrate that the model is highly significant ($p$<0.0001). With a coefficient of determination ($R^2$) of 0.9034, the model exhibits an excellent goodness-of-fit. Furthermore, the interaction terms $X_3X_8$, $X_3X_{10}$, $X_6X_{10}$, and $X_8X_{10}$ were found to significantly influence the angle of repose ($p$<0.05). The model's coefficient of variation (CV) of 5.73% indicates high precision and reliability in the experiment.

## 4.5 Interaction effects in the regression model

To intuitively analyze the impact of significant interaction terms on the angle of repose, response surface analysis plots were generated based on the regression equations (Figure 8). Figure 8a response surface shows a steeper slope in the $X_3$ direction than in the $X_8$ direction, indicating the stronger influence of $X_3$ as compared to $X_8$. In Figure 8b, the contour lines are denser along the $X_{10}$

**Table 8 BBD experimental design and results**

| Test No. | Factor | | | | Angle of repose/(°) |
|---|---|---|---|---|---|
| | $X_3$ | $X_6$ | $X_8$ | $X_{10}$ | |
| 1 | –1 | –1 | 0 | 0 | 27.33 |
| 2 | –1 | 0 | 1 | 0 | 33.87 |
| 3 | 0 | 1 | 0 | 1 | 30.58 |
| 4 | 0 | –1 | 0 | –1 | 27.25 |
| 5 | 0 | 0 | 0 | 0 | 26.53 |
| 6 | 0 | 0 | –1 | 1 | 39.54 |
| 7 | 1 | –1 | 0 | 0 | 37.63 |
| 8 | 0 | 0 | 1 | –1 | 31.97 |
| 9 | 0 | 0 | –1 | –1 | 25.92 |
| 10 | 1 | 0 | 0 | 1 | 34.83 |
| 11 | 0 | 0 | 1 | 1 | 34.59 |
| 12 | 0 | 0 | 0 | 0 | 29.94 |
| 13 | 0 | –1 | 1 | 0 | 35.83 |
| 14 | 1 | 0 | 1 | 0 | 31.92 |
| 15 | 0 | –1 | 0 | 1 | 39.77 |
| 16 | 0 | 0 | 0 | 0 | 31.98 |
| 17 | 1 | 0 | –1 | 0 | 38.63 |
| 18 | 0 | 1 | 0 | –1 | 28.36 |
| 19 | 0 | 0 | 0 | 0 | 27.56 |
| 20 | 1 | 0 | 0 | –1 | 32.71 |
| 21 | 0 | 0 | 0 | 0 | 30.72 |
| 22 | –1 | 1 | 0 | 0 | 27.87 |
| 23 | –1 | 0 | –1 | 0 | 31.43 |
| 24 | –1 | 0 | 0 | 1 | 37.54 |
| 25 | 1 | 1 | 0 | 0 | 31.61 |
| 26 | 0 | 1 | 1 | 0 | 30.54 |
| 27 | 0 | 1 | –1 | 0 | 30.45 |
| 28 | –1 | 0 | 0 | –1 | 25.78 |
| 29 | 0 | –1 | –1 | 0 | 36.28 |

**Table 9 Analysis of variance of regression model**

| Source | Sum of squares | *df* | Mean square | *F*-value | *p*-value | |
|---|---|---|---|---|---|---|
| Model | 440.99 | 14 | 31.50 | 9.35 | <0.0001 | ** |
| $X_3$ | 46.06 | 1 | 46.06 | 13.68 | 0.0024 | ** |
| $X_6$ | 50.76 | 1 | 50.76 | 15.07 | 0.0017 | ** |
| $X_8$ | 1.04 | 1 | 1.04 | 0.3084 | 0.5874 | |
| $X_{10}$ | 167.70 | 1 | 167.70 | 49.80 | <0.0001 | ** |
| $X_3X_6$ | 10.76 | 1 | 10.76 | 3.19 | 0.0955 | |
| $X_3X_8$ | 20.93 | 1 | 20.93 | 6.22 | 0.0258 | * |
| $X_3X_{10}$ | 23.23 | 1 | 23.23 | 6.90 | 0.0199 | * |
| $X_6X_8$ | 0.0729 | 1 | 0.0729 | 0.0216 | 0.8851 | |
| $X_6X_{10}$ | 26.52 | 1 | 26.52 | 7.88 | 0.0140 | * |
| $X_8X_{10}$ | 30.25 | 1 | 30.25 | 8.98 | 0.0096 | ** |
| $X_3^2$ | 17.19 | 1 | 17.19 | 5.10 | 0.0403 | * |
| $X_6^2$ | 2.93 | 1 | 2.93 | 0.8688 | 0.3671 | |
| $X_8^2$ | 52.88 | 1 | 52.88 | 15.70 | 0.0014 | ** |
| $X_{10}^2$ | 11.63 | 1 | 11.63 | 3.45 | 0.0842 | |
| Residual | 47.14 | 14 | 3.37 | | | |
| Lack of fit | 26.84 | 10 | 2.68 | 0.5290 | 0.8112 | |
| Pure error | 20.30 | 4 | 5.07 | | | |
| Cor total | 488.13 | 28 | | | | |

Note: *significant ($p$<0.05); **highly significant ($p$<0.01).

direction than along $X_3$, forming a distinct elliptical shape, which signifies the greater influence of $X_{10}$ than $X_3$. Similarly, Figures 8c and 8d demonstrate that $X_{10}$ also exerts a stronger effect on the angle of repose than $X_6$ and $X_8$. Collectively, the effects of all four interaction terms on the angle of repose were found to be significant ($p$<0.05). The order of interaction effect strength is as follows: $X_8X_{10} > X_6X_{10} > X_3X_{10} > X_3X_8$.

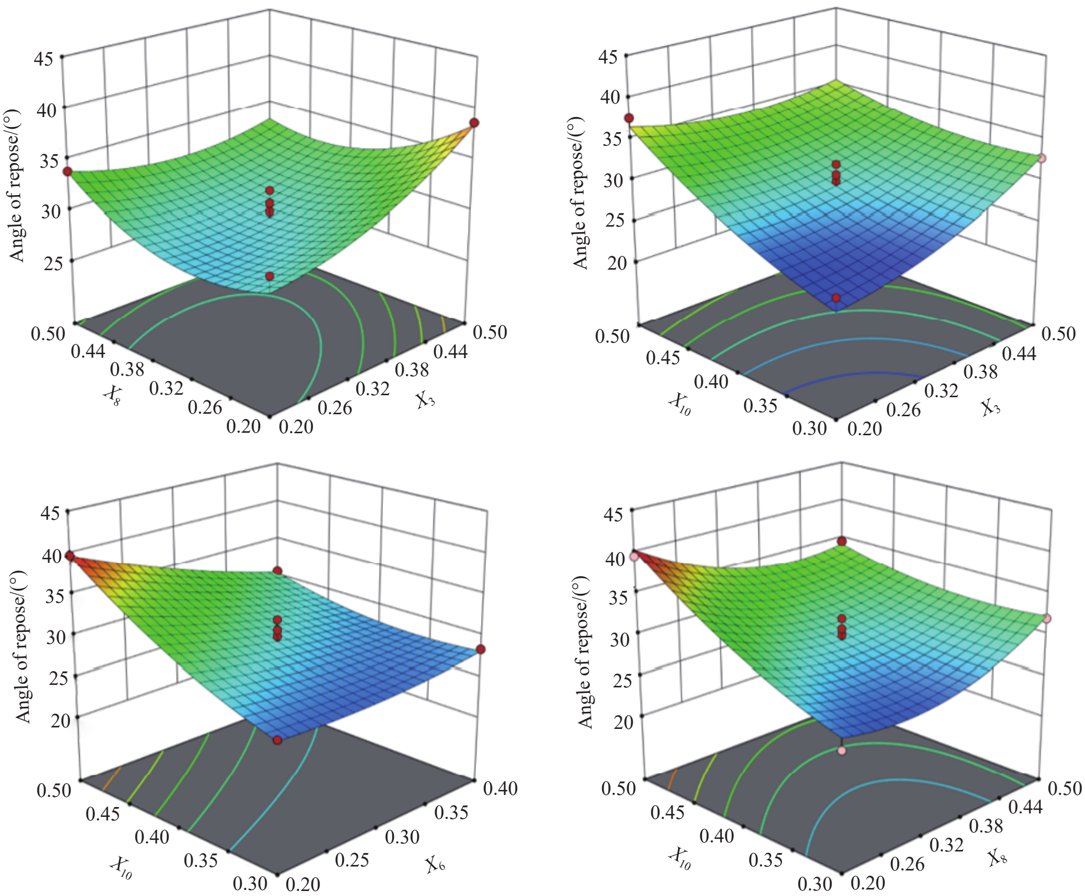


Figure 8 Interaction response surface plot

**4.6 Optimization of residual film-cotton stalk blending parameters and model validation**

4.6.1 Objective function and constraints

Within the specified factor level range, parameters were optimized using the Design-Expert software's optimization function. The model was solved with a target value of 31.59°, and multiple solution sets were simulated for verification. The solution set that most closely matched the physical test geometry was selected[30], yielding the following values: cotton stalk-residual film rolling friction coefficient: 0.46, residual film-residual film rolling friction coefficient: 0.31, residual film-steel rolling friction coefficient: 0.47, residual film-residual film JKR surface energy: 0.41 J/m$^2$.

4.6.2 Angle of repose verification test

The optimal parameters were set in EDEM, with other contact parameters configured at intermediate levels[31]. Figure 9 displays the discrete element simulation of the cotton stalk-residual film mixture's angle of repose. After repeating the test 10 times, the average simulated angle of repose was found to be 32.59°, with a relative error of 3.06% compared to the actual angle of repose. These results confirm the reliability of the calibrated contact parameters for the cotton stalk-residual film mixture.

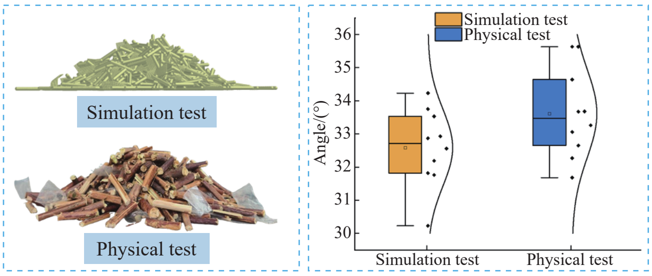


a. Simulation tests and physical tests b. Statistical analysis of test results

Figure 9 Comparison of physical test and simulation test of stacking angle

## 5 Conclusions

This study utilized physical testing methods, including inclined plane, three-point bending, and tensile load tests, to determine specific values for the coefficient of friction and coefficient of restitution. For parameters difficult to measure experimentally, their numerical ranges were established through a literature review. A custom-built test rig was employed to measure the angle of repose of the cotton stalk-residual film mixture. Using the angle of repose as the response variable, a significance analysis, screening, and optimization of the physical parameters for the cotton stalk-residual film mixture were performed using Plackett-Burman design, the steepest ascent method, and Box-Behnken response surface analysis. A simulation model for the angle of repose was then established based on the optimized parameters and validated against physical test results to verify the accuracy of the calibrated parameters. The specific conclusions of this study are as follows:

(1) For the discrete element simulation parameter calibration of the cotton stalk-residual film mixture, Plackett-Burman results indicate that the rolling friction coefficient between cotton stalks and residual film, the rolling friction coefficient between residual films, the residual film-to-steel rolling friction coefficient, and the residual film-to-residual film JKR surface energy significantly influence the mixture's angle of repose. Other simulation parameters showed no significant effect on the angle of repose.

(2) The secondary multiple regression model for the cotton stalk-residual film mixture exhibited reliable performance, as confirmed by results from steepest climb tests and Box-Behnken response surface experiments. The model identified the following parameter combinations as significantly influencing the mixture's angle of repose: cotton stalk-residual film rolling friction coefficient: 0.46; residual film-residual film rolling friction coefficient: 0.31; residual film-steel rolling friction coefficient: 0.47; residual film-residual film JKR surface energy: 0.41 J/m$^2$.

(3) EDEM simulation tests, utilizing calibrated parameters, yielded a simulated pile angle of 32.59° for the cotton stalk-residual film mixture, exhibiting a 3.06% deviation from the actual pile angle. Optimized calibration parameters can be employed to simulate the contact parameters of this mixture. It should be noted that the discrete element simulation model for the cotton stalk-residual film mixture established in this study shows certain discrepancies with the physically tested angle of repose. This discrepancy may arise from the simplification of cotton stalks into a uniform particle composition during model development, whereas actual cotton stalks possess distinct mechanical properties between their outer skin and inner core. Modeling with a single particle type inherently introduces errors. Therefore, future research could involve simulating the outer skin and inner core of cotton stalks using particles with distinct material properties, thereby creating a cotton stalk-residual film mixture model that more accurately reflects real-world conditions. Compared to Shen et al.[10] and Li et al.[11], who modeled single-component plastic film waste, this study focuses primarily on calibrating the contact parameters for a mixture of plastic film and cotton stalks, and validates the model. This will provide a reference for future studies on the interaction between cotton straw and residual film during the recovery process, and for the establishment of a residual film–cotton straw–soil complex.

## Acknowledgements

This research was supported by the Xinjiang Uygur Autonomous Region Key Research and Development Project (Grant No. 2022B02023-3), the Xinjiang Uygur Autonomous Region Competitive Bidding and Leadership Projects (Grant No. XJJBGS-MG202403), the Science and Technology Innovation Leading Talent Project of the Xinjiang Uygur Autonomous Region (Grant No. 2024TSYCLJ0014), the Xinjiang Agricultural University Graduate Research Innovation Project (Grant No. XJAUGRI2025011), and Science and Technology Support for Xinjiang Project (Grant No. 2026E02020).

## [References]

[1] Lu H Y, Chen W M, Wang F Y, Fu J H, Han H Y, Wan S M. Current situation of cotton straw returning and its influence on cotton growth and soil physical and chemical properties. China Cotton, 2025; 52(1): 8–12. (in Chinese) DOI: 10.11963/cc20240094

[2] Wei X, Zhang Y P, Pan Z L, Li P C, Sun G L, Wang J, et al. The current situation and research progress of comprehensive utilization of cotton straw. Chinese Journal of Eco-Agriculture, 2025; 33(7): 1245–1260. (in Chinese) DOI: 10.12357/cjea.20250096

[3] Wang Y, Sun Y W, Ye Z H, Chen Y Z, Li J. Research progress, prospects, and development countermeasures of cotton stalk utilization in China. China Cotton, 2025; 52(10): 71–78. (in Chinese) DOI: 10.11963/cc2024 0086

[4] Gao N, Zhu Z C, Han H Y, Zhang G J, Zhou J J, Lv D C, et al. Research on the recycling utilization of edible fungi cultivated as cotton by products in Xinjiang. Oasis Agriculture Science and Engineering, 2025; 10(2): 77–87. (in Chinese) DOI: 10.26941/j.cnki.2096-2177.2025.02.010

[5] Zhao H B, Wang X Z, Zheng Z Q, Li X H, Huang Y X. Research status

and progress of discrete element method applications in agricultural equipment. Transactions of the CSAM, 2025; 56(7): 1–19. (in Chinese) DOI: 10.6041/j.issn. 1000-1298.2025.07.001
[6] Shi R J, Dai F, Zhao W Y, Zhang F W, Shi L R, Guo J H. Establishment of discrete element flexible model and verification of contact parameters of flax stem. Transactions of the CSAM, 2022; 53(10): 146–155. (in Chinese) DOI: 10.6041/j.issn. 1000-1298.2022.10.015
[7] Du Z, Li D H, Li X P, Jin X, Wu Y B, Yu F. Calibration and experiment of discrete element model parameters for tea stem. Transactions of the CSAM, 2025; 56(1): 311–320. (in Chinese) DOI: 10.6041/j.issn. 1000-1298.2025.01.030
[8] Zhang J X, Zhang P, Zhang H, Tan C L, Wan W Y, Wang Y C. Discrete element simulation parameters calibration for Xinjiang cotton straw. Transactions of the CSAM, 2024; 55(1): 76–84, 108. (in Chinese) DOI: 10.6041/j.issn. 1000-1298.2024.01.007
[9] Shu C X, Yang J, Wan X Y, Yuan J C, Liao Y T, Liao Q X. Parameter calibration and experiment of the discrete element simulation parameters of rape threshing mixture in combine harvester. Transactions of the CSAE, 2022; 38(9): 34–43. (in Chinese)
[10] Shen S L, Zhang J X, Jiang Y X, Wang Y C, Liu X F, Li J M, et al. Tensile properties of residual film in tillage layer based on discrete element method. Transactions of the CSAM, 2024; 55(7): 132–141. (in Chinese) DOI: 10.6041/j.issn.1000-1298.2024.07.013
[11] Li J L, Wang X Z, Zhang B C, Feng Z, Meng H W, Kan Z. Construction method of flexible DEM model for agricultural residual film based on multi-feature comprehensive analysis. Transactions of the CSAM, 2025; 56(7): 170–179. (in Chinese) DOI: 10.6041/j.issn. 1000-1298.2025.07.015
[12] Liu X L, Shi R J, Zhao W Y, Sun W, Li P W, Li H, et al. Study on the characteristics of residual film-soil-root stubble complex in maize stubble fields of the Hexi corridor and establishment of a discrete element model. Agriculture, 2024; 14(9): 1542–1542.
[13] Deng H, Dai F, Shi R J, Song X F, Zhao W Y, Pan H F. Simulation of full-film double-row furrow roller hole fertilizer application based on DEM-MBD coupling and research on its water and fertilizer transport law. Biosystems Engineering, 2024; 239: 190–206.
[14] Fang W Q, Wang X Z, Han D L, Zang N, Chen X G, Ohiemi I E. Parameter optimization and disturbance analysis of the film pickup device of the chain-type plough layer residual film recycling machine based on DEM-MBD coupling. Computers and Electronics in Agriculture, 2024; 222: 109041.
[15] Tian X L, Cong X, Qi J T, Guo H, Li M, Fan X H. Parameter calibration of discrete element model for corn straw-soil mixture in black soil areas. Transactions of the CSAM, 2021; 52(10): 100–108, 242. (in Chinese) DOI: 10.6041/j.issn. 1000-1298.2021.10.010
[16] Ma Y C, Qi Y, Wang H Y, Teng D, Chen J Q, Liu D. Discrete element simulation parameter calibration and experiment of corn straw-cow manure mixture. Transactions of the CSAM, 2024; 55(12): 441–450, 504. (in Chinese) DOI: 10.6041/j. issn. 1000-1298.2024. 12.042
[17] Guo H, Han J X, Lv Z S, Dong Y D, Guo L H, Zhou W. Discrete element model construction and parameter calibration of combined harvest oil sunflower extract. Transactions of the CSAM, 2025; 56(5): 319–330. (in Chinese) DOI: 10.6041/j.issn. 1000-1298.2025.05.030
[18] Zhang Z G, Zeng C, Xing Z Y, Xu P, Guo Q F, Shi R M, et al. Discrete element modeling and parameter calibration of safflower biomechanical properties. Int J Agric & Biol Eng, 2024; 17(2): 72–81.
[19] Sun K, Yu J Q, Zhao J W, Sun Y C, Yu Y J, Liang L S, et al. Parameter calibration and experimental validation of wheat straw model for cutting process simulation. Transactions of the CSAM, 2025; 56(7): 116–127. (in Chinese) DOI: 10.6041/j. issn. 1000-1298.2025.07.010
[20] Li Y Z, Xie J H, Zhang J, Yue Y, Meng Q H, Du Y K, et al. Parameter calibration and experimental verification of discrete element simulation model for protaetia brevitarsis larvae bioconversion mixture. Int J Agric & Biol Eng, 2024; 17(4): 35–44.
[21] Chen F, Yang L, Cui T, Zhang D X, He X T, Zhang K L. Establishment and parameter calibration of the discrete element model for typical clay in hilly and mountainous areas. Int J Agric & Biol Eng, 2025; 18(5): 26–38.
[22] Xia J F, Zhang P, Yuan H W, Du J, Zheng K, Li Y F. Calibration and verification of flexible rice straw model by discrete element method. Transactions of the CSAM, 2024; 55(9): 174–184. (in Chinese) DOI: 10.6041/j.issn.1000-1298.2024.09.014
[23] Zhang W J, Jiang S C, Kong X R, Geng J, Niu Z Y, Li H C. Analysis of impact characteristics of hammermill screen based on discrete element method and calibration of contact parameters of crushed particles. Transactions of the CSAM, 2025; 56(4): 501–511. (in Chinese) DOI: 10.6041/j.issn.1000-1298.2025.04.047
[24] Zhang H J, Han X, Yang H W, Chen X B, Zhao G Z, Sun J W, et al. Calibrating and simulating contact parameters of the discrete element for apple particles. Transactions of the CSAE, 2024; 40(12): 66–76. (in Chinese) DOI: 10.11975/j.issn.1002-6819.202312100
[25] Wang F A, Zeng Y, Zhang Z G, Xie K T, Li D H, He Z P. Parameter calibration of discrete element simulation model for *panax notoginseng* planting soil. Journal of South China Agricultural University, 2024; 45(4): 588–597. (in Chinese) DOI: 10.7671/i.issn.1001-411X.202309042
[26] Xie W, Ouyang C, Jiang P, Meng D X, Luo H F. Calibrating and optimizing the discrete element parameters for clamping section stems during rape shoot harvesting. Transactions of the CSAE, 2024; 40(7): 104–116. (in Chinese) DOI: 10.11975/j.issn.1002-6819.202310041
[27] Cui T, Jing M S, Zhang D X, Yang L, He X T, Wang Z D. Construction of the discrete element model for maize ears and verification of threshing simulation. Transactions of the CSAE, 2023; 39(24): 33–46. (in Chinese) DOI: 10.11975/j.issn.1002-6819.202307199
[28] Peng Q J, He X, Li G M, Yang R S, Wang X Y, Zhang C Y, et al. Calibrating and testing the discrete element parameters for peanut seedling film. Int J Agric & Biol Eng, 2024; 17(5): 65–72.
[29] Chen Y, Gao X X, Jin X, Ma X R, Hu B, Zhang X L. Calibration and analysis of seeding parameters of *cyperus esculentus* seeds based on discrete element simulation. Transactions of the CSAM, 2023; 54(12): 58–69. (in Chinese) DOI: 10.6041/j.issn.1000-1298.2023.12.005
[30] Xiao W L, Liao Q X, Liao Y T, Wang L, Wan X Y. Discrete elemental parameter calibration of the bonding model for caking compound fertilizer utilized in oilseed rape mechanized direct seeding. Int J Agric & Biol Eng, 2025; 18(4): 17–25.
[31] Li J M, Zhang J X, Wang Y C, Gao Z B, Wang X X, Shen S L. Calibration of parameters for a discrete element model of cotton field residual film-soil mixtures. Int J Agric & Biol Eng, 2026; 19(1): 59–66.